

Non-global logarithms up to four loops at finite- N_c for V/H+jet processes at hadron colliders

Kamel Khelifa-Kerfa

*Department of Physics, Faculty of Science and Technology
Université de Relizane, Relizane 48000, Algeria*

*Laboratoire de Mathématique et Applications,
Université Hassiba BenBouali de Chlef, Chlef 02000, Algeria*

E-mail: kamel.khelifakerfa@univ-relizane.dz

ABSTRACT: We extend our previous work [1] on calculating non-global logarithms in e^+e^- annihilation to Higgs/vector boson production in association with a single hard jet at hadron colliders. We analytically compute non-global coefficients in the jet mass distribution up to four loops using the anti- k_t jet algorithm. Our calculations are performed in the eikonal approximation, assuming strong energy ordering for the emitted gluons, thus capturing only the leading logarithms of the distribution. We compare our analytical results with the all-orders large- N_c numerical solution. In general, the gross features of the non-global logarithm distribution observed in the e^+e^- case remain valid for the V/H+jet processes.

KEYWORDS: QCD, Resummation, Jets, LHC, Higgs, Eikonal

Contents

1	Introduction	1
2	Definitions and kinematics	3
2.1	Hadronic processes	3
2.2	Observable definition	4
2.3	Jet mass distribution	6
3	NGLs calculations	7
3.1	NGLs at 2-loops	7
3.2	NGLs at 3-loops	10
3.3	NGLs at 4-loops	13
4	Comparisons to all-orders results	15
4.1	Conformal transformation	18
5	Conclusion	20
A	4-loops calculations	22

1 Introduction

In the endeavour of enhancing the possibility of disentangling new physics signals from those that are purely background, jet substructure techniques have played a central role, particularly at hadron colliders such as the current highest-energy CERN Large Hadron Collider (LHC). This is mainly due to the fact that at such colliders, final-state particles, including those resulting from the decay of Beyond Standard Model (BSM) heavy particles, are produced highly collimated and will most likely be reconstructed by jet algorithms into a single jet. Not only this, but jet substructure has also aided in the scrutiny of the Standard Model (SM) itself, especially in threshold phase space regions. Moreover, it has helped in initiating relatively new computational techniques in the field of high-energy physics, such as Machine Learning, as well as in providing a common ground for both theorists and experimentalists to enrich their interactions and discussions (see, for instance, Ref. [2] for an experimental review and Ref. [3] for a theoretical review of jet substructure).

Amongst the widely studied jet substructures/shapes, both in e^+e^- and hadron collisions, is the invariant mass of a jet m_j . It is an infrared and collinear safe observable that is sensitive to soft and collinear emissions from both initial- and final-state partons, and thus important as a probe of various QCD aspects such as colour flow, hadronisation, underlying events, large logarithms, to name a few. It is part of a large class of observables, called *non-global* [4, 5], that are sensitive to specific regions of phase space. These latter observables

are notorious for giving rise to single logarithms¹ and beyond, in their perturbative series, known as *non-global logs* (NGLs), which are generally large and hence unavoidable for any precision calculation. They manifest the non-abelian nature of QCD and have not been fully understood despite the significant efforts by the jet substructure community (see, for example, [6–14] and references in [3]). Their state-of-the-art resummation is next-to-leading NGLs in the large- N_c limit [15, 16] (N_c is the number of quark colours).

In the context of higher-order calculations, we computed in Ref. [1] NGL coefficients that are present in the hemisphere mass distribution in e^+e^- collisions fully up to 4-loops and partially through 5-loops. The calculations included full colour dependence, instead of the large- N_c approximation that had been previously widely used. They were performed in the eikonal (soft) approximation and thus only guaranteed single logarithmic accuracy. We then computed NGLs up to 2-loops for hadron collisions in the anti- k_t algorithm [17] in Ref. [12] (Z +jet and dijet events), then in the k_t [18, 19] and Cambridge-Aachen (C-A) [20] algorithms in Ref. [21] (Higgs/vector boson + jet events).

In the present paper, we generalise the work of [1] in a number of ways: first, we study the invariant mass of the leading- p_t jet, instead of the hemisphere mass, and second, we consider scattering processes at hadron colliders, instead of e^+e^- annihilation. These generalisations make the current work much more subtle than that of [1], due to the complexity of hadronic scattering environments (including initial-state radiation (ISR), parton distribution functions (PDFs), multiple emission dipoles, etc.), the presence of the jet radius parameter R in all calculations, the various Born channels for a given process, to name a few. The specific hadronic processes that we shall be treating are the production of a Higgs boson H or a vector boson (Z, W^\pm or γ) in association with a single hard jet j . The state-of-the-art fixed-order QCD calculations for these processes are next-to-next-to-leading-order (NNLO) [22–28]. The resummation of NGLs at hadron colliders has only been performed numerically at large- N_c in the anti- k_t jet algorithm [12] using the Monte Carlo (MC) program developed in [4].

We follow the procedure outlined in [1] by implementing the eikonal approximation and assuming strong energy-ordering of the transverse momenta of the radiated gluons; $p_t \gg k_{t1} \gg \dots \gg k_{tn}$. This facilitates the computation of both real emission amplitudes and their corresponding virtual corrections. The general formalism as well as the detailed explicit formulae (up to 4-loops) for the eikonal amplitudes squared for the hadronic processes considered herein have been presented in our recent paper [29]. The latter paper represents a generalisation of the previous e^+e^- calculations of eikonal amplitudes squared [30]. Furthermore, we apply the *measurement operator*, first introduced in [14], to write the integrals of the NGL coefficients in a finite manner. The said integrals are then performed analytically whenever possible via a series expansion in the jet radius R , otherwise, we resort to multi-dimensional libraries, such as Cuba [31, 32], to compute them numerically. The final results for each Born channel are presented for 2-, 3-, and 4-loops. It is worth

¹These are of the form $\alpha_s^n L^n$ where n is an integer, α_s is the strong coupling constant, and L is a large logarithm of the ratio of m_j to another hard scale in the process, usually the transverse momentum of the jet p_t or the centre-of-mass energy Q .

noting that all results shown herein are for the anti- k_t jet algorithm. Similar calculations of NGLs in other jet algorithms will be presented elsewhere [33].

This paper is organised as follows. In sec. 2, we present the details of the hadronic processes considered, including the various Born channels, recall the definition of the jet mass observable, the anti- k_t jet algorithm, and the general formula of the jet mass distribution. After briefly reviewing the calculations at 1-loop, which have been performed previously (see for instance [12] and [21]), in sec. 3, we present the details of the calculations of NGL coefficients at 2-, 3-, and 4-loops. Moreover, comparisons of both the exponential and expansion forms of our NGL calculations to the all-orders large- N_c results from [12] and the MC program [4] are carried out in sec. 4. These will be used to hint at the significance of the finite- N_c corrections as well as that of the missing higher-order terms. Finally, we conclude in sec. 5.

2 Definitions and kinematics

The problem that we treat in this work is the computation of NGLs at single logarithmic accuracy that appear in the distribution of the invariant mass of the leading hard jet produced in association with a Higgs or one of the vector bosons, Z, W or γ , at hadron colliders. We shall adopt the notation used in our recent paper [21] which dealt with the same observable and for the same processes (but only for up to 2-loops). We note that for QCD calculations all bosons are considered as (colour-neutral) singlets and thus do not explicitly enter the NGLs calculations. Therefore, all aforementioned processes are, at the parton level, of the type of three-hard coloured QCD partons/legs considered in [29]. They may only differ in the specific Born channels. We further note that all hard partons are considered massless.

2.1 Hadronic processes

For the vector boson ($Z/W/\gamma$) + jet processes there are three Born channels that contribute to the scattering amplitude, namely:

$$(\delta_1) : q\bar{q} \rightarrow g + V, \quad (\delta_2) : qg \rightarrow q + V \quad (2.1a)$$

and $\bar{q}g \rightarrow \bar{q}$, where V refers to one of the vector (colour-neutral) bosons Z, W or γ . The latter channel is in fact identical to (δ_1) in terms of colour flow (which along with the Born cross section are the only distinguishing factors between all channels) and hence will not explicitly be considered further. The particular details of the production of W^\pm , which involves flavour changing, are too not relevant for our QCD NGLs calculations. Furthermore, the Higgs + jet production has in addition to the above mentioned three channels a fourth one, namely the all-gluons channel

$$(\delta_3) : gg \rightarrow g + H. \quad (2.1b)$$

Fig. 1 shows the Feynman diagrams corresponding to the above three Born channels.

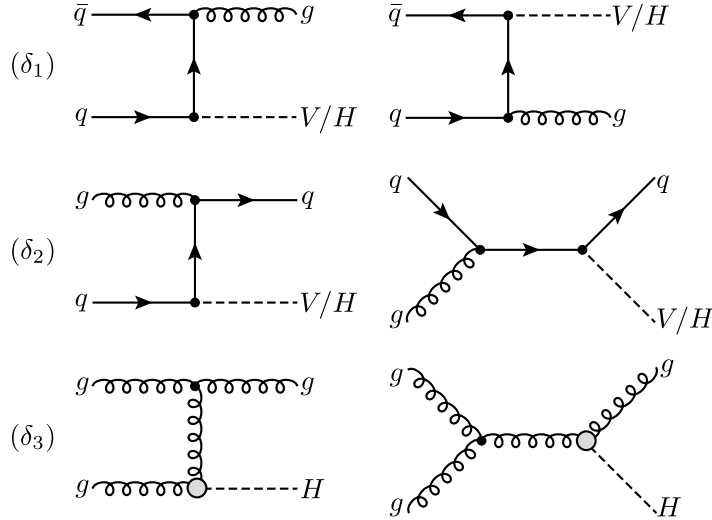


Figure 1: Feynman diagrams for the three Born channels contributing to hadronic processes considered in the current work (figure from [21]).

2.2 Observable definition

At the parton level we schematically represent the scattering process for the various Born channels mentioned above in association with the emission of n soft gluons g_i as

$$a(p_a) + b(p_b) \rightarrow j(p_j) + X + g_1(k_1) + \cdots + g_n(k_n), \quad (2.2)$$

where a and b label the incoming hard partons, j the outgoing hard parton initiating the leading hard jet, X the Higgs or V bosons, and p_i and k_ℓ the corresponding four-momenta of the i^{th} hard parton (a , b or j) and the ℓ^{th} soft gluon, respectively. The explicit expressions of the latter momenta are given by:

$$p_a = x_a \frac{\sqrt{s}}{2} (1, 0, 0, 1), \quad (2.3a)$$

$$p_b = x_b \frac{\sqrt{s}}{2} (1, 0, 0, -1), \quad (2.3b)$$

$$p_j = p_t (\cosh y, \cos \varphi, \sin \varphi, \sinh y), \quad (2.3c)$$

$$k_i = k_{ti} (\cosh \eta_i, \cos \phi_i, \sin \phi_i, \sinh \eta_i), \quad (2.3d)$$

where p_t , y and φ are the transverse momentum, rapidity and azimuthal angle of outgoing final-state hard jet, and k_{ti} , η_i and ϕ_i are the transverse momentum, rapidity and azimuthal angle of the i^{th} soft emission, measured with respect to the beam axis. The collision centre-of-mass energy is \sqrt{s} and x_a, x_b are the momentum fractions carried by the incoming beam partons a and b , respectively. Worth mentioning is that the effect of recoil of hard partons against soft emissions is beyond single logarithmic accuracy (see for instance Ref. [34]) and will thus be neglected throughout.

The (squared) invariant mass of the leading hard jet normalised to the its transverse momentum p_t is given by the sum of the momenta of the hard outgoing massless parton

j and the final-state soft emissions k_i that end up inside the jet after applying the jet algorithm. That is:

$$\begin{aligned} \varrho &= \frac{m_j^2}{p_t^2} = \frac{1}{p_t^2} \left(p_j + \sum_{i \in j} k_i \right)^2 = \sum_{i \in j} \varrho_i + \mathcal{O} \left(\frac{k_t^2}{p_t^2} \right), \\ \varrho_i &= \frac{2(p_j \cdot k_i)}{p_t^2} = \frac{2k_{ti}}{p_t} [\cosh(\eta_i - y) - \cos(\phi_i - \varphi)], \end{aligned} \quad (2.4)$$

where in the soft limit one neglects terms that are proportional to k_t^2 .

The detailed recipe of the three well-known jet algorithms is well explained, for example, in [21]. The anti- k_t jet algorithm works, in the strong-energy ordering regime, in a simple manner. In the (η, ϕ) plane, one draws a circle of radius R around the hard outgoing parton j . Any soft emission k_i that resides inside this circle will be recombined with the latter jet, otherwise it will not. The momentum of the resultant jet will be the sum of the momenta of the constituent partons. Soft gluons that are not clustered as part of the said hard jet may be clustered with other gluons, if they are within a radius of R from each other, otherwise they will be considered as separate final state jets. Mathematically, a soft gluon k_i is considered inside the jet if the following condition is satisfied

$$(y - \eta_i)^2 + (\varphi - \phi_i)^2 < R^2. \quad (2.5)$$

As mentioned above, (2.4), only partons that are clustered with the hard jet contribute to its mass. The emergence of NGLs for the jet mass observable has been extensively discussed in prior literature (see, for example, [1, 10–12]). Essentially, the phenomenon begins with the radiation of two soft gluons, k_1 and k_2 , from one of the Born configurations, Eqs. (2.1a) and (2.1b). The first, harder gluon k_1 , emitted outside the jet, subsequently emits the second, softer real gluon k_2 into the jet vicinity (see Fig. 2). This gluon k_2 then contributes to the mass of the jet. However, if gluon k_2 is virtual, it cannot be clustered with the jet and thus does not contribute to its mass. This scenario results in an incomplete cancellation between real and virtual contributions to the jet mass observable, leaving large logarithmic terms in the jet mass.

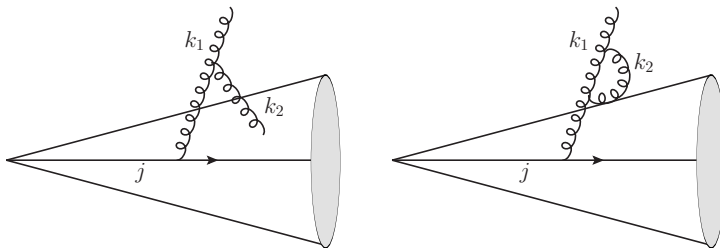


Figure 2: A schematic diagram showing how NGLs arise at 2-loops.

The details of the various configurations that give rise to NGLs at 2-, 3- and 4-loops have been thoroughly discussed in our previous work [1] and shall not be repeated herein. The interested reader is referred to the latter reference for more information. The expressions

of the integrals of the NGLs coefficients at a given order in the perturbation expansion of the jet mass will be identical to those presented in the said reference for the same order (more details later).

A parametrisation in terms of the polar variables (r, θ) that will prove useful in performing NGLs integrals is given by

$$\eta_i - y = Rr_i \cos \theta_i, \quad \phi_i - \varphi = Rr_i \sin \theta_i, \quad (2.6)$$

where $r_i > 0$, $2\pi > \theta_i > 0$ and $d\eta_i d\phi_i = R^2 r_i dr_i d\theta_i$. The anti- k_t clustering condition (2.5) reduces, in the latter parametrisation, to the simple form:

$$k_i \in j \quad \Rightarrow \quad r_i < 1. \quad (2.7)$$

Moreover, the normalised jet mass (2.4) may be expanded as a series in R . That is:

$$\varrho_i = \xi_i \left[R^2 r_i^2 + \frac{1}{12} R^4 r_i^4 \cos(2\theta_i) + \frac{1}{960} R^6 r_i^6 \cos(4\theta_i) + \dots \right]. \quad (2.8)$$

For the accuracy level of our calculations, which is single log, it suffices to only keep the first term in the above expansion. Hence, in the remaining of the paper, we shall assume, unless stated otherwise, that

$$\varrho_i \approx \xi_i R^2 r_i^2. \quad (2.9)$$

2.3 Jet mass distribution

The differential cross-section for the distribution of the normalised invariant jet mass may be written, for a specific channel δ , as

$$\frac{d\Sigma_\delta(\rho)}{d\mathcal{B}_\delta} = \int_0^\rho \frac{d^2\sigma_\delta}{d\mathcal{B}_\delta d\varrho} d\varrho, \quad (2.10)$$

where \mathcal{B}_δ denotes the Born configuration with a differential element given by $d\mathcal{B}_\delta = dx_a dx_b f_a(x_a, \mu_F^2) f_b(x_b, \mu_F^2)$, where f_i is the PDF of the i^{th} incoming parton and μ_F is the factorisation scale (see appendix A of Ref. [21] for full details). In the small mass region, $\rho \ll 1$, where large logarithms dominate the distribution, the differential cross-section (2.10) may be cast in the form

$$\frac{d\Sigma_\delta(\rho)}{d\mathcal{B}_\delta} = \frac{d\sigma_{0,\delta}}{d\mathcal{B}_\delta} f_{\mathcal{B},\delta}(\rho) [1 + \mathcal{O}(\alpha_s)], \quad (2.11)$$

where $d\sigma_{0,\delta}/d\mathcal{B}_\delta$ is the partonic differential cross-section for the Born channel δ (discussed in depth in appendix A of [21]). The function $f_{\mathcal{B},\delta}(\rho)$ resums all various large logarithms appearing in the ρ -distribution. It may be written in the factorised form

$$f_{\mathcal{B},\delta}(\rho) = f_{\mathcal{B},\delta}^{\text{global}}(\rho) \mathcal{S}_\delta(\rho), \quad (2.12)$$

where $f_{\mathcal{B},\delta}^{\text{global}}(\rho)$ represents the well-known Sudakov form factor that results from the exponentiation of the single-gluon emission. It accounts for soft- and hard-collinear radiations

off the outgoing jet as well as soft wide-angle primary (non-correlated) radiations from all hard partons (incoming and outgoing). It may be written, up to NLL, as [12, 21]:

$$f_{\mathcal{B},\delta}^{\text{global}}(\rho) = \frac{e^{-\mathcal{R}_\delta(\rho) - \gamma_E \mathcal{R}'_\delta(\rho)}}{\Gamma[1 + \mathcal{R}'_\delta(\rho)]}, \quad (2.13)$$

where $\gamma_E \approx 0.577$ and the various terms have been defined and fully computed in [12] with their explicit expressions presented in the appendix C of the said reference and appendix B of [21].

In the current paper we are interested in the term $\mathcal{S}_\delta(\rho)$ which represents the resummation of leading (single) NGLs. Its fixed-order series expansion may be written as

$$\mathcal{S}_\delta(\rho) = 1 + \mathcal{S}_{2,\delta}(\rho) + \mathcal{S}_{3,\delta}(\rho) + \mathcal{S}_{4,\delta}(\rho) + \dots. \quad (2.14)$$

In what follows below we will be carrying out detailed calculations of the first three NGLs contributions above. i.e., at 2-, 3- and 4-loops.

3 NGLs calculations

3.1 NGLs at 2-loops

As we mentioned above, the integrals of the NGLs coefficients for our hard processes assume the same forms as those encountered in e^+e^- calculations [1]. In other words, the 2-loops NGLs integral reads

$$\mathcal{S}_{2,\delta}(\rho) = - \int_{\xi_1 > \xi_2} d\Pi_{12} \Xi^{\text{anti-}k_t}(k_1, k_2) \overline{\mathcal{W}}_{12,\delta}^{\text{RR}}, \quad (3.1)$$

where $\xi_i = k_{ti}/p_t$ and $\Xi^{\text{anti-}k_t}(k_1, k_2)$ is the constraint resulting from the application of the anti- k_t algorithm. It reads

$$\begin{aligned} \Xi^{\text{anti-}k_t}(k_1, k_2) &= \Theta[(\eta_1 - y)^2 + (\phi_1 - \varphi)^2 - R^2] \Theta[R^2 - (\eta_2 - y)^2 - (\phi_2 - \varphi)^2], \\ &\equiv \Theta_1^{\text{out}} \Theta_2^{\text{in}}. \end{aligned} \quad (3.2)$$

The 2-loops phase space factor $d\Pi_{12} = d\Phi_1 d\Phi_2 \Theta(\varrho_1 - \rho) \Theta(\varrho_2 - \rho)$ where the 1-loop phase space factor is given by

$$d\Phi_i = \bar{\alpha}_s \frac{d\xi_i}{\xi_i} d\eta_i \frac{d\phi_i}{2\pi}, \quad (3.3)$$

with $\bar{\alpha}_s = \alpha_s/\pi$. The (*irreducible* part) of the eikonal amplitude squared $\overline{\mathcal{W}}_{12,\delta}^{\text{RR}}$ appearing in (3.1) is given in [29]:

$$\overline{\mathcal{W}}_{12,\delta}^{\text{RR}} = C_A \sum_{(ij) \in \Delta_\delta} \mathcal{C}_{ij} \mathcal{A}_{ij}^{12}, \quad (3.4)$$

where the sum is over all possible dipoles formed by the partons in the Born channel δ . That is, $\Delta_\delta = \{(aj), (bj), (ab)\}$. The dipole colour factor \mathcal{C}_{ij} have been discussed in Refs. [29] and [30]. They read:

$$\mathcal{C}_{q\bar{q}} = \mathcal{C}_{qq} = 2C_F - C_A, \quad \mathcal{C}_{gg} = \mathcal{C}_{gq} = C_A, \quad (3.5)$$

where $C_F = (N_c^2 - 1)/2N_c$ and $C_A = N_c$ are the colour Casimir scalars for (anti)quarks and gluons, respectively. The 2-loops antenna function \mathcal{A}_{ij}^{12} is defined, in a general form, as

$$\mathcal{A}_{\alpha\beta}^{ij} = w_{\alpha\beta}^i (w_{\alpha i}^j + w_{i\beta}^j - w_{\alpha\beta}^j), \quad (3.6)$$

where $w_{\alpha\beta}^i$ is the 1-loop dipole antenna function defined by ²

$$w_{\alpha\beta}^i = \frac{k_{ti}^2}{2} \frac{(p_\alpha \cdot p_\beta)}{(p_\alpha \cdot k_i)(k_i \cdot p_\beta)}. \quad (3.7)$$

Notice that both the 1-, and 2-loops antenna functions are purely angular functions. That is, they depend neither on the colour flow nor on the four momenta.

Substituting Eqs. (3.2), (3.3) and (3.4) back into the integral of the 2-loops NGLs coefficient (3.1) we have

$$\begin{aligned} \mathcal{S}_{2,\delta}(\rho) = & -C_A \sum_{(ij) \in \Delta_\delta} \mathcal{C}_{ij} \bar{\alpha}_s^2 \int_{\xi_1 > \xi_2} \frac{d\xi_1}{\xi_1} \frac{d\xi_2}{\xi_2} d\eta_1 d\eta_2 \frac{d\phi_1}{2\pi} \frac{d\phi_2}{2\pi} \Theta_1^{\text{out}} \Theta_2^{\text{in}} \times \\ & \times \Theta(\varrho_1 - \rho) \Theta(\varrho_2 - \rho) \mathcal{A}_{ij}^{12}. \end{aligned} \quad (3.8)$$

In order to perform the above integration we use the change of variables (2.6) and the accompanying approximations (2.7) and (2.9), to write

$$\begin{aligned} \mathcal{S}_{2,\delta}(\rho) = & -C_A \sum_{(ij) \in \Delta_\delta} \mathcal{C}_{ij} \bar{\alpha}_s^2 R^4 \int_{\xi_1 > \xi_2} \frac{d\xi_1}{\xi_1} \frac{d\xi_2}{\xi_2} r_1 dr_1 r_2 dr_2 \frac{d\theta_1}{2\pi} \frac{d\theta_2}{2\pi} \Theta(r_1 - 1) \Theta(1 - r_2) \times \\ & \times \Theta(\xi_1 r_1^2 R^2 - \rho) \Theta(\xi_2 R^2 r_2^2 - \rho) \mathcal{A}_{ij}^{12}. \end{aligned} \quad (3.9)$$

Up to single log accuracy, i.e., keeping only the leading NGLs, the energy ξ 's integrals factorise out to give $L^2/2!$ where $L = \ln(R^2/\rho)$. We may then write the 2-loops NGLs contribution as:

$$\mathcal{S}_{2,\delta}(\rho) = -\frac{1}{2!} \bar{\alpha}_s^2 L^2 \mathcal{G}_{2,\delta}(R), \quad (3.10)$$

where the NGLs coefficient

$$\begin{aligned} \mathcal{G}_{2,\delta}(R) = & C_A \sum_{(ij) \in \Delta_\delta} \mathcal{C}_{ij} R^4 \int_1^{\frac{\pi}{R|\sin\theta_1|}} r_1 dr_1 \int_0^{2\pi} \frac{d\theta_1}{2\pi} \int_0^1 r_2 dr_2 \int_0^{2\pi} \frac{d\theta_2}{2\pi} \mathcal{A}_{ij}^{12}, \\ = & C_A \sum_{(ij) \in \Delta_\delta} \mathcal{C}_{ij} \mathcal{I}_{ij}(R). \end{aligned} \quad (3.11)$$

Few points to mention regarding the above integral. First, up to single log accuracy the lower limit on r_2 's integral, which is $\sqrt{\rho/R^2}$, has been set to 0 since the 2-loops antenna function \mathcal{A}_{ij}^{12} is finite. Second, the upper limit on the r_1 integral comes from the fact that $(\phi_1 - \varphi) \in [-\pi, \pi]$ and from Eq. (2.6) it follows that $\pi/(R \sin \theta_1) > r_1 > -\pi/(R \sin \theta_1)$. Since $r_1 > 1$ (from anti- k_t clustering condition (2.7)) and $\sin \theta_1$ changes its sign over the range $[0, 2\pi]$ one finds the upper limit shown in Eq. (3.11).

The procedure that we shall follow to do the angular integrals $\mathcal{I}_{ij}(R)$ of Eq. (3.11), as well as the corresponding integrals at 3- and 4-loops, is as follows:

²Note that compared to the definitions of the phase space factor and the 1-loop antenna function in [29] a factor of 1/2 has been moved from the former to the latter in the present paper.

1. Compute the integral for each dipole (ij) separately.
2. Substitute the parametrisation (2.6) into the expression of the angular integrand (the 2-loops antenna function \mathcal{A}_{ij}^{12} in (3.11)) and expand it as a series in R .
3. Whenever the upper limit is of the form $\pi/(R|\sin\theta|)$ then split the integration range into two regions: (a) $1 < r < \pi/R$, and (b) $\pi/R < r < \pi/(R|\sin\theta|)$.
4. Sum up the contributions from all regions.

We note that all of our analytical series results for all integrals have been verified numerically using, as stated above, **Cuba** library. We find the following expressions for the NGLs coefficients \mathcal{I}_{ij} for the (incoming-jet) dipole, labelled as (aj) or (bj), and (incoming-incoming) dipole, labelled as (ab), dipoles:

$$\mathcal{I}_{aj} = \mathcal{I}_{bj} = \frac{\zeta_2}{2} + 0.003 R^4 + \mathcal{O}(R^8), \quad (3.12a)$$

$$\mathcal{I}_{ab} = \frac{1}{2} R^2 (1 - 2 \ln R) + \frac{1}{8} R^4 - 0.003 R^6 + \mathcal{O}(R^8). \quad (3.12b)$$

Fig. 3 shows comparisons between the analytical series above, (3.12a) and (3.12b), and the pure numerical integration results. Our findings agree with those reported previously [12, 21]. Substituting Eqs. (3.12a) and (3.12b) back into the expression of $\mathcal{G}_{2,\delta}$ (3.11) and

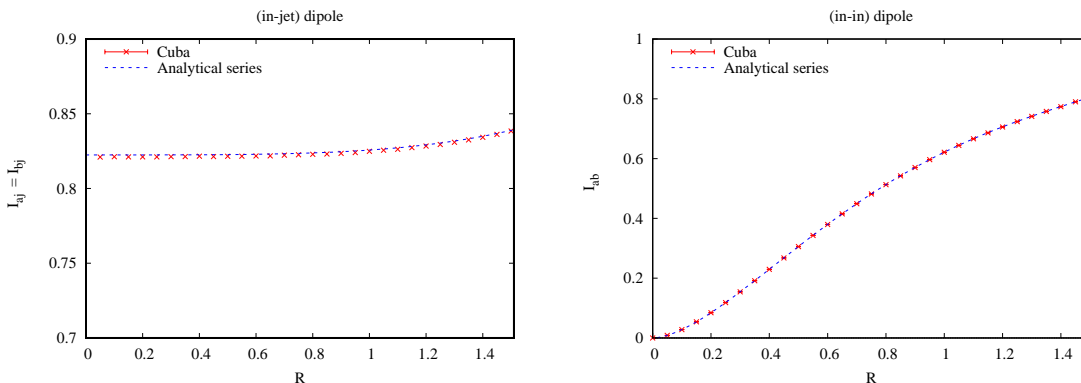


Figure 3: Comparisons between analytical and numerical results for the NGLs coefficients 2-loops.

simplifying we obtain the following formulae for each of the three channels:

$$\mathcal{G}_{2,\delta_1}(R) = C_F C_A [1.645 + 0.007 R^4] + C_A^2 [0.5 R^2 - R^2 \ln(R) + 0.125 R^4 - 0.003 R^6] + \mathcal{O}(R^8), \quad (3.13a)$$

$$\mathcal{G}_{2,\delta_2}(R) = C_F C_A [R^2 - 2 R^2 \ln(R) + 0.25 R^4 - 0.007 R^6] + C_A^2 [1.645 - 0.5 R^2 + R^2 \ln(R) - 0.118 R^4 + 0.003 R^6] + \mathcal{O}(R^8), \quad (3.13b)$$

$$\mathcal{G}_{2,\delta_3}(R) = C_A^2 [1.645 + 0.5 R^2 - R^2 \ln(R) + 0.132 R^4 - 0.003 R^6] + \mathcal{O}(R^8). \quad (3.13c)$$

In Fig. 4 we show the NGLs coefficients (3.13) for all three channels. Clearly the contri-

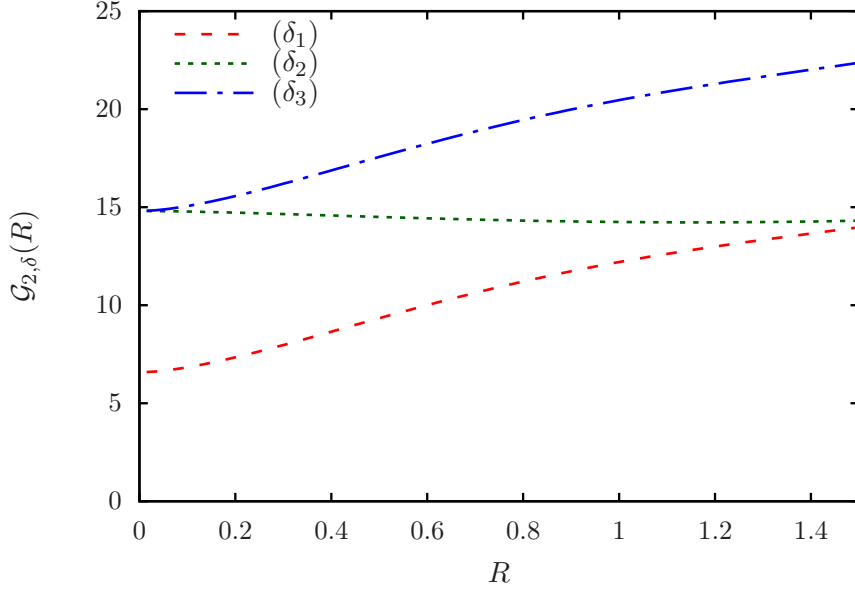


Figure 4: NGLs coefficients at 2-loops for all of the three Born channels.

bution of channel (δ_3) is the largest due to the colour factor. Note that in the limit $R \rightarrow 0$ one finds for the above NGLs coefficients:

$$\lim_{R \rightarrow 0} \mathcal{G}_{2,\delta_1}(R) = C_F C_A \zeta_2, \quad \lim_{R \rightarrow 0} \mathcal{G}_{2,\delta_2}(R) = C_A^2 \zeta_2, \quad \lim_{R \rightarrow 0} \mathcal{G}_{2,\delta_3}(R) = C_A^2 \zeta_2, \quad (3.14)$$

where $\zeta_2 = 1.645$. i.e., one recovers the results found in e^+e^- hemisphere mass distribution [1, 4]. This is due to the fact that NGLs arise predominantly at the boundary of the phase space region of interest. In other words, as far as the jet region, the phase space region relevant to our jet mass observable, has a boundary (or edge) even if it is vanishingly small then NGLs effects will be present.

The calculations presented thus far, for NGLs at 2-loops, are not entirely new and have already been presented in the literature. It is the 3- and 4-loops calculations, discussed in the next sections, that are new and presented herein for the first time in the literature.

3.2 NGLs at 3-loops

The 3-loops NGLs integral is given in an identical form to that presented in the e^+e^- case [1] (Eq. (3.10)). That is,

$$\mathcal{S}_{3,\delta}(\rho) = - \int_{\xi_1 > \xi_2 > \xi_3} d\Pi_{123} \Theta_1^{\text{out}} \Theta_3^{\text{in}} \left(\Theta_2^{\text{in}} \overline{\mathcal{W}}_{123,\delta}^{\text{RVR}} + \Theta_2^{\text{out}} \left[\overline{\mathcal{W}}_{123,\delta}^{\text{RVR}} + \overline{\mathcal{W}}_{123,\delta}^{\text{RRR}} \right] \right), \quad (3.15)$$

where as before $d\Pi_{123} = \prod_{i=1}^3 d\Phi_i \Theta(\varrho_i - \rho)$, with the 1-loop phase space factor given in (3.3), and the eikonal amplitudes squared are given in Ref. [29]. They read

$$\overline{\mathcal{W}}_{123,\delta}^{\text{RRR}} = C_A^2 \sum_{(ij) \in \Delta_\delta} \mathcal{C}_{ij} [\mathcal{A}_{ij}^{12} \overline{\mathcal{A}}_{ij}^{13} + \mathcal{B}_{ij}^{123}] + Q_\delta \sum_{\pi_{\{ijk\}}} [\mathcal{G}_{ij}^{k1}(2,3) + 2 \leftrightarrow 3], \quad (3.16a)$$

$$\overline{\mathcal{W}}_{123,\delta}^{\text{RVR}} = -C_A^2 \sum_{(ij) \in \Delta_\delta} \mathcal{C}_{ij} \mathcal{A}_{ij}^{12} \overline{\mathcal{A}}_{ij}^{13} - Q_\delta \sum_{\pi_{\{ijk\}}} [\mathcal{G}_{ij}^{k1}(2,3) + 2 \leftrightarrow 3], \quad (3.16b)$$

where $\overline{\mathcal{A}}_{ij}^{k\ell} = \mathcal{A}_{ij}^{k\ell}/w_{ij}^k$, the permutation $\pi_{\{ijk\}} = \{(ijk), (ikj), (jki)\}$, the 3-loops antenna function $\mathcal{B}_{\alpha\beta}^{ijk}$ and the *quadruple* function $\mathcal{G}_{ij}^{k\ell}$ are defined by

$$\mathcal{B}_{\alpha\beta}^{ijk} = w_{\alpha\beta}^i \left(\mathcal{A}_{\alpha i}^{jk} + \mathcal{A}_{i\beta}^{jk} - \mathcal{A}_{\alpha\beta}^{jk} \right), \quad (3.17a)$$

$$\mathcal{G}_{ij}^{k\ell}(n, m) = w_{ij}^\ell T_{ij}^{k\ell}(n) U_{ij}^{k\ell}(m), \quad (3.17b)$$

with $T_{ij}^{k\ell}(n) = w_{ij}^n + w_{k\ell}^n - w_{ik}^n - w_{j\ell}^n$ and $U_{ij}^{k\ell}(n) = w_{ij}^n + w_{k\ell}^n - w_{i\ell}^n - w_{jk}^n$. The quadrupole colour factor Q_δ reads

$$Q_{\delta_1} = Q_{\delta_2} = C_A^2 (C_A - 2C_F) = C_A, \quad Q_{\delta_3} = 6 C_A. \quad (3.18)$$

Substituting all of the above expressions back into the formula of $\mathcal{S}_{3,\delta}(\rho)$ (3.15) we find that, just like the 2-loops integral, up to single log accuracy the energy integrals factorise out to give $L^3/3!$. We then write the NGLs contribution at 3-loops in an analogous form to (3.10):

$$\mathcal{S}_{3,\delta}(\rho) = +\frac{1}{3!} \bar{\alpha}_s^3 L^3 \mathcal{G}_{3,\delta}(R), \quad (3.19)$$

where

$$\mathcal{G}_{3,\delta}(R) = C_A^2 \sum_{(ij) \in \Delta_\delta} \mathcal{C}_{ij} \left(\mathcal{J}_{ij}^{(1)}(R) - \mathcal{J}_{ij}^{(2)}(R) \right) + 2Q_\delta \sum_{(ijk) \in \pi_\delta} \mathcal{J}_{ijk}^{(3)}(R), \quad (3.20)$$

with $\pi_\delta = \{(ajb), (bj a), (abj)\}$, the factor of 2 in the second part of the rhs of the above equation comes from the $(2 \leftrightarrow 3)$ symmetry of the integrand and the integral expressions of the various terms in (3.20) are given by

$$\mathcal{J}_{ij}^{(1)}(R) = R^6 \int_0^{2\pi} \prod_{i=1}^3 \frac{d\theta_i}{2\pi} \int_1^{\frac{\pi}{R|\sin\theta_1|}} r_1 dr_1 \int_0^1 r_2 dr_2 \int_0^1 r_3 dr_3 \mathcal{A}_{ij}^{12} \overline{\mathcal{A}}_{ij}^{13}, \quad (3.21a)$$

$$\mathcal{J}_{ij}^{(2)}(R) = -R^6 \int_0^{2\pi} \prod_{i=1}^3 \frac{d\theta_i}{2\pi} \int_1^{\frac{\pi}{R|\sin\theta_1|}} r_1 dr_1 \int_1^{\frac{\pi}{R|\sin\theta_2|}} r_2 dr_2 \int_0^1 r_3 dr_3 \mathcal{B}_{ij}^{123}, \quad (3.21b)$$

$$\mathcal{J}_{ijk}^{(3)}(R) = R^6 \int_0^{2\pi} \prod_{i=1}^3 \frac{d\theta_i}{2\pi} \int_1^{\frac{\pi}{R|\sin\theta_1|}} r_1 dr_1 \int_0^1 r_2 dr_2 \int_0^1 r_3 dr_3 \mathcal{G}_{ij}^{k1}(2,3). \quad (3.21c)$$

Following the procedure outlined at 2-loops one can find an analytical R -series expansion for all of the three integrals. They read

$$\mathcal{J}_{aj}^{(1)} = \mathcal{J}_{bj}^{(1)} = \zeta_3 + \frac{1}{16} R^2 + 0.005 R^4 - 0.001 R^6 - \mathcal{O}(R^8), \quad (3.22a)$$

$$\mathcal{J}_{ab}^{(1)} = \zeta_2 R^2 + \frac{1}{2} R^4 (\ln R - 1) - \frac{1}{32} R^6 - \mathcal{O}(R^8). \quad (3.22b)$$

for the first part,

$$\mathcal{J}_{aj}^{(2)} = \mathcal{J}_{bj}^{(2)} = \frac{\zeta_3}{2} + \frac{1}{16}R^2 - 0.017R^4 + 0.012R^6 - \mathcal{O}(R^8), \quad (3.23a)$$

$$\mathcal{J}_{ab}^{(2)} = R^2(\ln^2 R - \ln R + 0.5) - (0.652 \ln R - 0.375)R^4 + (0.051 \ln R - 0.004)R^6 - \mathcal{O}(R^8), \quad (3.23b)$$

for the second part, and for the third part we sum up the three contributions $\mathcal{J}_{ajb}^{(3)} + \mathcal{J}_{bja}^{(3)} + \mathcal{J}_{abj}^{(3)}$, since the colour factor Q_δ is independent of the choice of the triplets (ajb) , (bja) and (abj) , to give a *cross-channel* coefficient

$$\mathcal{J}_X^{(3)} = \frac{1}{4}R^2 + R^4(0.125 \ln R - 0.022) - 0.023R^6 + \mathcal{O}(R^8). \quad (3.23c)$$

Substituting the various formulae above back into the form of $\mathcal{G}_{3,\delta}(R)$ (3.20) we can deduce the expression of the latter for each channel. To this end we have:

$$\begin{aligned} \mathcal{G}_{3,\delta_1}(R) &= C_F C_A^2 [1.202 - R^2 + (0.09 - 0.5 \ln R)R^4 + 0.094R^6] + \\ &+ C_A^3 [(1.645 + \ln R - \ln^2 R)R^2 + (1.402 \ln R - 0.919)R^4 - \\ &- (0.073 + 0.051 \ln R)R^6] + \mathcal{O}(R^8), \end{aligned} \quad (3.24a)$$

$$\begin{aligned} \mathcal{G}_{3,\delta_2}(R) &= C_F C_A^2 [(1.29 + 2 \ln R - 2 \ln^2 R)R^2 + (1.805 \ln R - 1.662)R^4 + \\ &+ (0.039 - 0.103 \ln R)R^6] + \\ &+ C_A^3 [1.202 + (\ln^2 R - \ln R - 0.645)R^2 + (0.838 - 0.902 \ln R)R^4 + \\ &+ (0.051 \ln R - 0.018)R^6] + \mathcal{O}(R^8), \end{aligned} \quad (3.24b)$$

$$\begin{aligned} \mathcal{G}_{3,\delta_3}(R) &= C_A^3 [1.202 + (1.145 + \ln R - \ln^2 R)R^2 + (1.152 \ln R - 0.868)R^4 - \\ &- (0.025 + 0.051 \ln R)R^6] + C_A [3R^2 + (1.5 \ln R - 0.264)R^4 - 0.279R^6] + \\ &+ \mathcal{O}(R^8). \end{aligned} \quad (3.24c)$$

In Fig. 5 we plot the above NGLs coefficients for all of the three channels. As expected, the large contribution comes from channel (δ_3) as it has a larger colour factor. Channel (δ_2) , just as observed at 2-loops, has its NGLs coefficient almost constant over the entire range of values of the jet radius R . In the limit $R \rightarrow 0$ one finds for the above NGLs coefficients

$$\lim_{R \rightarrow 0} \mathcal{G}_{3,\delta_1}(R) = C_F C_A^2 \zeta_3, \quad \lim_{R \rightarrow 0} \mathcal{G}_{3,\delta_2}(R) = C_A^3 \zeta_3, \quad \lim_{R \rightarrow 0} \mathcal{G}_{3,\delta_3}(R) = C_A^3 \zeta_3, \quad (3.25)$$

where $\zeta_3 = 1.202$. A similar result, to channel (δ_1) , has been found in e^+e^- hemisphere mass distribution [1]. This confirms, at 3-loops, the boundary nature of NGLs seen at 2-loops.

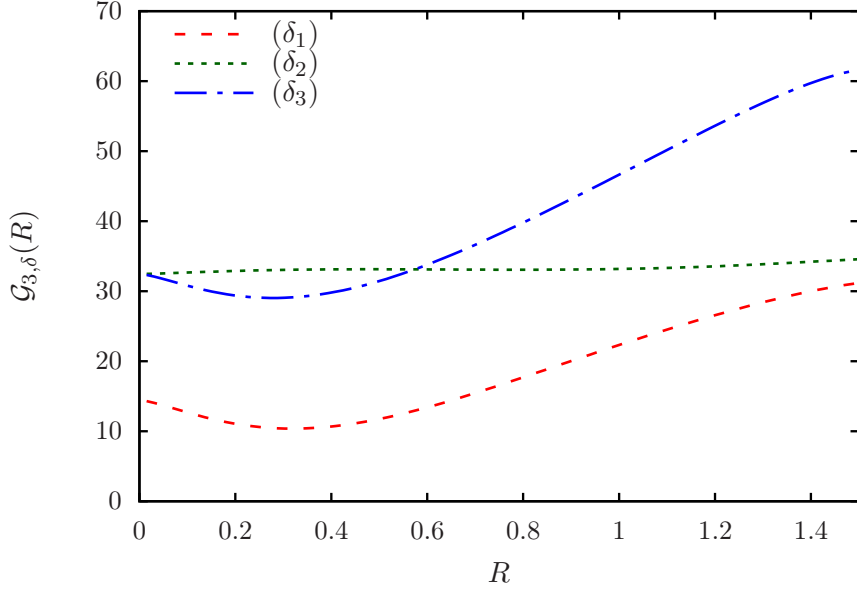


Figure 5: NGLs coefficients at 3-loops for all of the three Born channels.

3.3 NGLs at 4-loops

The expression of NGLs at 4-loops is, once again, analogous to that presented in [1] (Eqs. (3.21) and (3.22)). We write it in the form where all terms are separately finite as:

$$\begin{aligned}
\mathcal{S}_{4,\delta}(\rho) = & - \int_{\xi_1 > \dots > \xi_4} d\Pi_{1234} \Theta_1^{\text{out}} \Theta_4^{\text{in}} \times \left[\Theta_2^{\text{in}} \Theta_3^{\text{in}} \overline{\mathcal{W}}_{1234,\delta}^{\text{RVVR}} + \right. \\
& + \Theta_2^{\text{in}} \Theta_3^{\text{out}} \left(\overline{\mathcal{W}}_{1234,\delta}^{\text{RVVR}} + \overline{\mathcal{W}}_{1234,\delta}^{\text{RVRR}} \right) + \Theta_2^{\text{out}} \Theta_3^{\text{in}} \left(\overline{\mathcal{W}}_{1234,\delta}^{\text{RVVR}} + \overline{\mathcal{W}}_{1234,\delta}^{\text{RRVR}} \right) \\
& \left. + \Theta_2^{\text{out}} \Theta_3^{\text{out}} \left(\overline{\mathcal{W}}_{1234,\delta}^{\text{RVVR}} + \overline{\mathcal{W}}_{1234,\delta}^{\text{RVRR}} + \overline{\mathcal{W}}_{1234,\delta}^{\text{RRVR}} + \overline{\mathcal{W}}_{1234,\delta}^{\text{RRRR}} \right) \right]. \quad (3.26)
\end{aligned}$$

The expressions of the various eikonal amplitudes squared in the above formula are given in [29] and will not, for brevity, be explicitly repeated here. It is worth mentioning that all of the eikonal amplitudes above contain quadrupole (proportional to the quadrupole colour factor Q_δ (3.18)) terms that have some special features not seen in other terms (see Ref. [29, 30] for details). The latter terms were referred to as *ghost terms* in [30] and they correspond to: $\overline{\mathcal{N}}_{1234}^{\text{RRRR}}$, $\overline{\mathcal{N}}_{1234}^{\text{RVRR}}$, $\overline{\mathcal{N}}_{1234}^{\text{RRVR}}$ and $\overline{\mathcal{N}}_{1234}^{\text{RVVR}}$. Their corresponding expressions have not been written in an analytical closed form due to them being very cumbersome. Nonetheless, they may be integrated out easily.

Following the 2- and 3-loops calculations we write the 4-loops NGLs contribution (3.26) in the form

$$\mathcal{S}_{4,\delta}(\rho) = -\frac{1}{4!} \bar{\alpha}_s^4 L^4 \mathcal{G}_{4,\delta}(R), \quad (3.27)$$

where the NGLs coefficient at this order reads

$$\begin{aligned} \mathcal{G}_{4,\delta}(R) = C_A^3 \sum_{(ij) \in \Delta_\delta} C_{ij} \left[-\mathcal{K}_{ij}^{(1)} + \mathcal{K}_{ij}^{(3)} + \mathcal{K}_{ij}^{(5)} + \mathcal{K}_{ij}^{(6)} + \frac{Q_\delta}{C_A^3} \mathcal{K}_{ij}^{(7)} - \mathcal{K}_{ij}^{(9)} \right] - \\ - C_A Q_\delta \left[\mathcal{K}_X^{(2)} + \mathcal{K}_X^{(4)} + \mathcal{K}_X^{(8)} \right]. \end{aligned} \quad (3.28)$$

The integral expressions of the various terms in the above equation are reported in appendix A (Eqs. (A.1)). The results of integration of each term are also presented in the same appendix. For the reasons stated in the appendix we report here the numerical values of the NGLs coefficients $\mathcal{G}_{4,\delta}(R)$ for the three channels. They are plotted in Fig. 6. In the

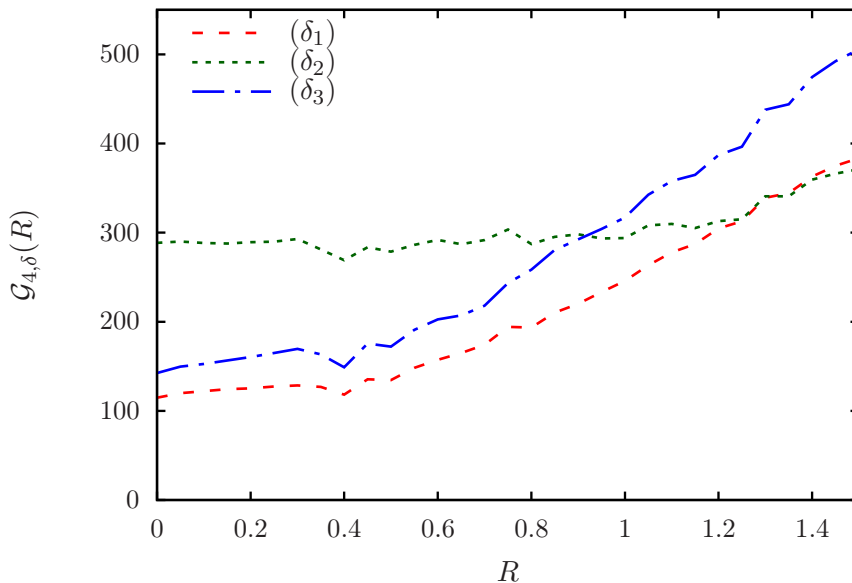


Figure 6: NGLs coefficients at 4-loops for all of the three Born channels.

limit $R = 0$ we have the explicit expressions of the latter coefficients given by:

$$\lim_{R \rightarrow 0} \mathcal{G}_{4,\delta_1}(R) = 1.08 C_F^2 C_A^2 + 8.79 C_F C_A^3 - 2.7 C_A^4, \quad (3.29a)$$

$$\lim_{R \rightarrow 0} \mathcal{G}_{4,\delta_2}(R) = 6.49 C_F C_A^3 + 0.678 C_A^4, \quad (3.29b)$$

$$\lim_{R \rightarrow 0} \mathcal{G}_{4,\delta_3}(R) = -19.5 C_A^2 + 3.92 C_A^4, \quad (3.29c)$$

Note that $\zeta_4 = 1.08$ and recall the e^+e^- result for the 4-loops coefficient [1]: $(25/8 C_F C_A^3 + C_F^2 C_A^2) \zeta_4 = 1.08 C_F^2 C_A^2 + 3.38 C_F C_A^3$. Thus in the limit $R \rightarrow 0$ the 4-loops NGLs coefficients in V/H+jet processes do not reduce to those of e^+e^- . The source of the mismatch is the contribution $\mathcal{K}_X^{(8)}$, and in particular the quadrupole ghost term $\bar{\mathcal{N}}_{1234}^{\text{RRVR}}$. It was shown in [30] that such terms, whereby both gluons 1 and 2 are *real*, possess very peculiar features, such as breaking both mirror and Bose symmetries (full details are to be found in the said

reference). As a confirmation to this observation, the other quadrupole contributions in Eq. (3.28), namely $\mathcal{K}_X^{(2)}$ and $\mathcal{K}_X^{(4)}$, tend to zero in the limit $R \rightarrow 0$, and hence do not contribute to the mismatch mentioned above. Evidently, none of them contains a term with both gluons 1 and 2 real.

To assess the accuracy of our calculations up to 4-loops, we shall carry out, in the next section, comparisons to the numerical all-orders large- N_c results presented in Ref. [12].

4 Comparisons to all-orders results

NGLs at hadron colliders have only been resummed numerically at large- N_c and in the anti- k_t jet algorithm using the MC code of [4], as reported in our previous work [12]. In the latter reference we used the following parametrisation, which includes the full contribution at 2-loops:

$$\mathcal{S}_\delta^{\text{MC}}(t) = \exp \left[-C_A \sum_{(ij) \in \Delta_\delta} \mathcal{C}_{ij} \mathcal{I}_{ij} f_{ij}(t) \right], \quad (4.1)$$

where \mathcal{I}_{ij} are the 2-loops NGLs coefficients reported in Eqs. (3.12a) and (3.12b) and

$$f_{ij}(t) = \frac{1 + (\lambda_{ij}t)^2}{1 + (\sigma_{ij}t)^{\gamma_{ij}}} t^2, \quad t = -\frac{1}{4\pi\beta_0} \ln(1 - 2\alpha_s(p_t)\beta_0 L). \quad (4.2)$$

Before proceeding further we note that according to the definitions of Ref. [12] the colour factors \mathcal{C}_{ij} there equal half their values here, and \mathcal{I}_{ij} there equal 4 times their values here. The functional form (4.1) is then fitted to the output of the MC code for each of the dipoles (ij) and the values of the fitting parameters $\lambda_{ij}, \sigma_{ij}$ and γ_{ij} are given in appendix C of [12]. We shall only consider two values of R , namely 0.7 and 1.0, for our comparisons. For the said values the fitting parameters are:

$$R = 0.7 : \quad \lambda_{aj} = \lambda_{bj} = 0.79C_A, \sigma_{aj} = \sigma_{bj} = 0.82C_A, \gamma_{aj} = \gamma_{bj} = 1.33, \\ \lambda_{ab} = 0.96C_A, \sigma_{ab} = 0.29C_A, \gamma_{ab} = 1.33, \quad (4.3a)$$

$$R = 1.0 : \quad \lambda_{aj} = \lambda_{bj} = 0.86C_A, \sigma_{aj} = \sigma_{bj} = 0.85C_A, \gamma_{aj} = \gamma_{bj} = 1.33, \\ \lambda_{ab} = 1.24C_A, \sigma_{ab} = 0.80C_A, \gamma_{ab} = 1.33. \quad (4.3b)$$

Note that at fixed order the evolution parameter t in Eq. (4.2) reduces to $\bar{\alpha}_s L/2$. We compare (4.1) to the exponential of our analytical NGLs results. That is:

$$\mathcal{S}_\delta(t) = \exp \left[-\frac{1}{2!} \mathcal{G}_{2,\delta}(R)(2t)^2 + \frac{1}{3!} \mathcal{G}_{3,\delta}(R)(2t)^3 - \frac{1}{4!} \mathcal{G}_{4,\delta}(R)(2t)^4 \right], \quad (4.4)$$

In Fig. 7 we plot the NGLs resummed factor (4.1) along with our analytical exponential factor (4.4) for $R = 0.7$ and $R = 1.0$ in all three Born channels. The solid lines represent the full expression (4.4) including finite- N_c contributions, whilst dashed lines represent the expression (4.4) in the large- N_c limit. i.e., the limit $C_F \rightarrow C_A/2$. The label ‘‘2-loops’’ means that we truncate the expression in the exponent (4.4) at t^2 , ‘‘3-loops’’ at t^3 and so

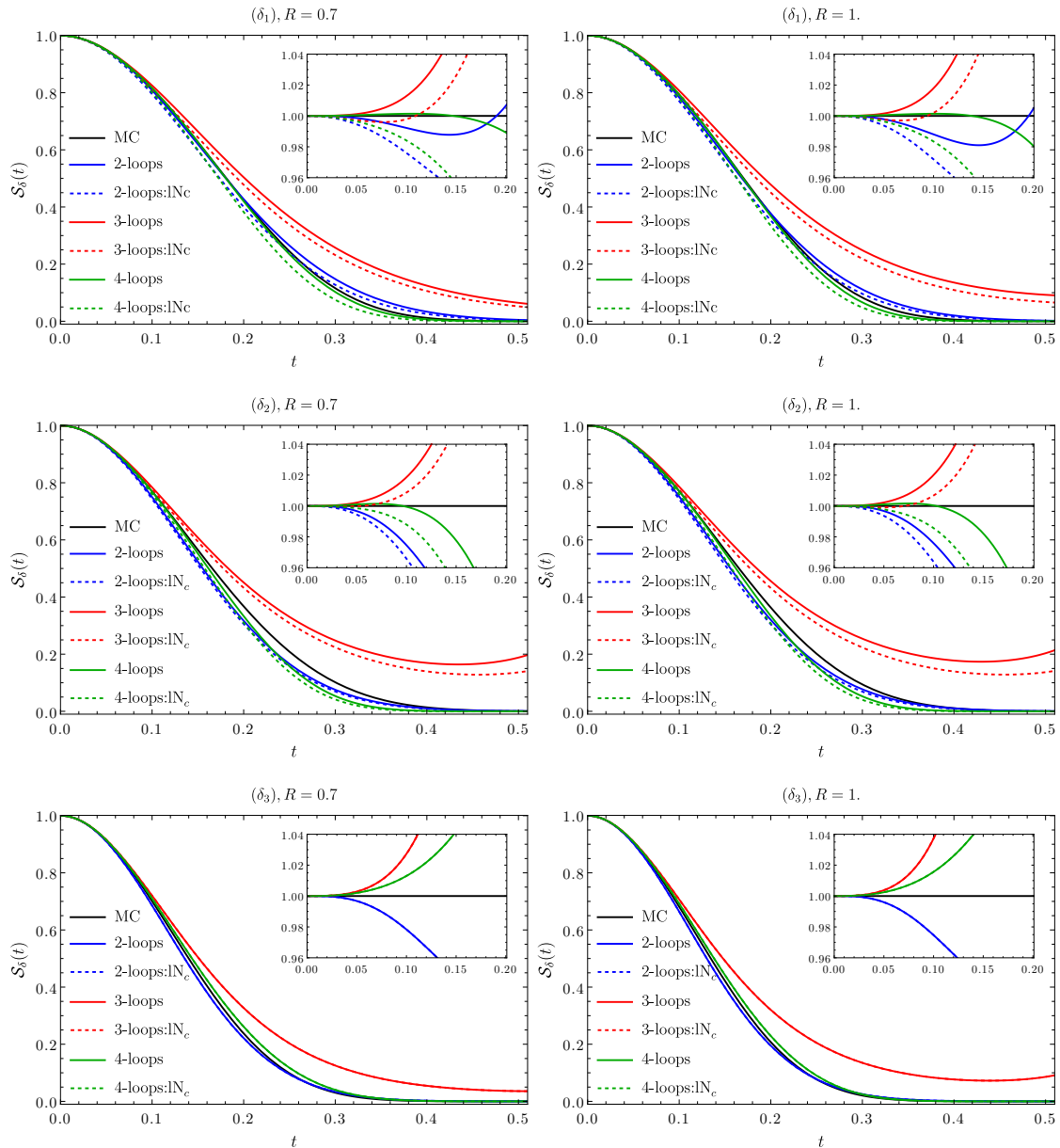


Figure 7: Comparisons between the all-orders large- N_c MC result and the exponential of our analytical calculations (4.4) for $R = 0.7$ (left) and $R = 1.0$ (right), for all three Born channels. Solid lines represent full colour contributions while dashed lines (with the abbreviation “lNc” for large- N_c) represent large- N_c contributions only.

on. Moreover, Fig. 9 is analogous to Fig. 7 except that it corresponds to comparisons of (4.1) and the power series expansion of (4.4).

Concerning the exponential form (Fig. 7), overall, the 2- and 4-loops curves seem to better represent the all-orders MC curve for the whole range of t . Zooming in one observes that, for smaller values of t , the 4-loops curve has a complete overlapping with the MC result over a slightly larger range of t than the 2- and 3-loops curves, particularly for channels

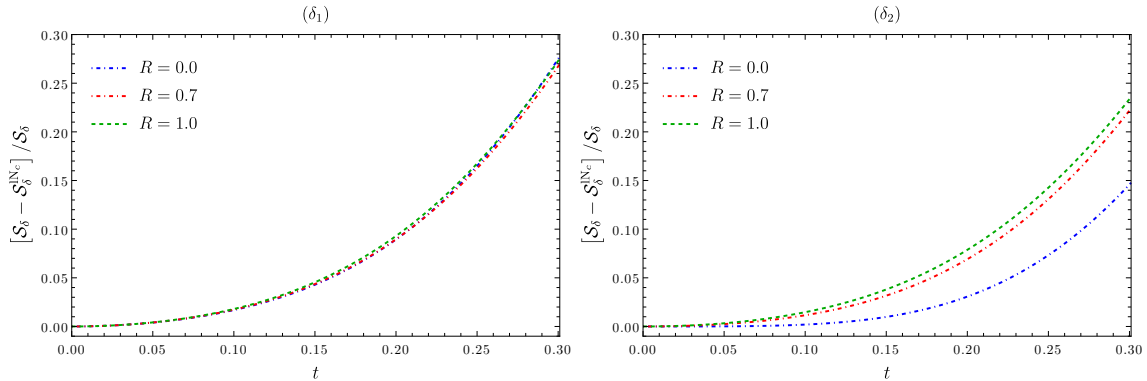


Figure 8: Comparisons between the analytical form factor (4.4) with (\mathcal{S}_δ) and without ($\mathcal{S}_\delta^{\text{N}_c}$) the finite- N_c contributions for all three jet radii, and for (left) channel (δ_1), and (right) channel (δ_2).

(δ_1) and (δ_2). A difference of less than 10% is achieved for values of t reaching out to about 0.2, or even higher for some cases, for both jet radii and for all Born channels, with the 4-loops performing better in most cases. The dependence on the jet radius R seems not to be significant. Moreover, the 2-loops exponential factor seems to approximate the all-orders to a good extent for all channels and all jet radii (this observation has been reported previously [1, 10]).

Furthermore, curves which include the finite- N_c contributions perform better than those that do not include them, especially for the 2- and 4-loops. This is true for channels (δ_1) and (δ_2) where quarks are present. The pure gluonic channel (δ_3) exhibits no difference between the two cases. In Fig. 8 we plot the percentage difference for the exponential form factor (4.4) with and without finite- N_c contribution for all three jet radii and for the aforementioned two channels. The difference ranges from about 0.4% at $t \sim 0.05$ up to more than 24% at $t \sim 0.3$ for both channels and most jet radii.

Concerning the power series expansion, we observe, from Fig. 9, that the higher the truncation order the better the agreement with the all-orders MC curve. This is evident in the zoomed-in plots, again especially for the first and second channels ((δ_1) and (δ_2)). Compared to the exponential form, the agreement is slightly worse and over a smaller range of t . We shall see in the next section that this behaviour might be significantly improved by applying some carefully chosen conformal transformations. As for the comparison between the full and large- N_c curves, similar features to those highlighted in the exponential case are observed.

It has been shown by e^+e^- fixed-order calculations of NGLs up to 12-loops in the large- N_c limit [35] as well as arguments based on the analytic structure of the large- N_c Banfi-Marchesini-Smye (BMS) equation [7] that NGLs series has a radius of convergence of about 1 (in the log defined in Ref. [14]) [36]. This corresponds, in our calculations, to $t \leq 1/(2N_c) \approx 0.17$. Thus, NGLs series distribution in V/H+jet processes at hadron colliders seems to have the same gross features seen in e^+e^- collisions.

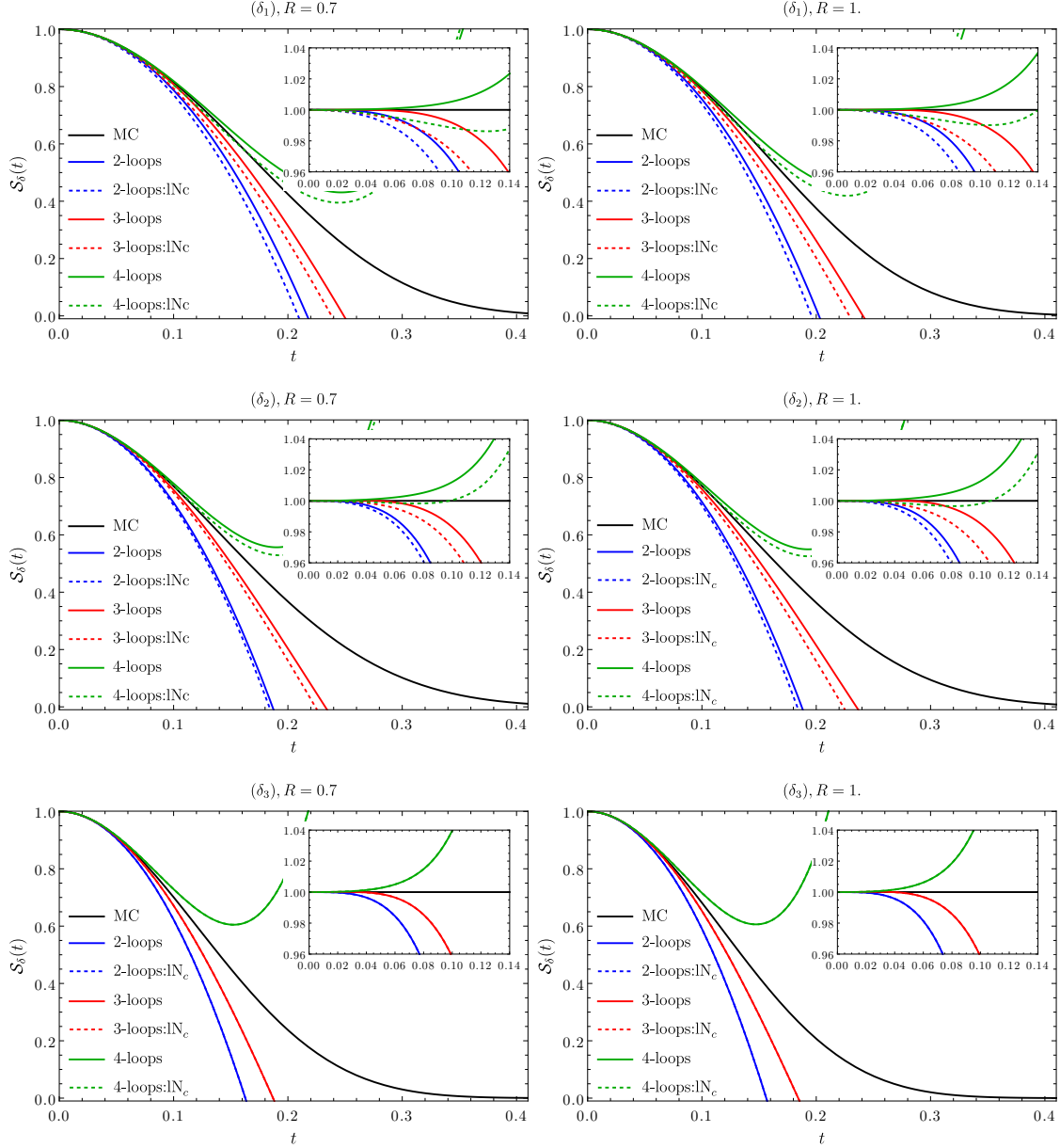


Figure 9: Comparisons between the all-orders large- N_c MC result and the power series expansion of the exponential form (4.4) for $R = 0.7$ (left) and $R = 1.0$ (right), for all three Born channels. Solid lines represent full colour contributions while dashed lines (with the abbreviation “lNc” for large- N_c) represent large- N_c contributions only.

4.1 Conformal transformation

In order to improve the convergence of the analytical power series expansion (towards the all-orders solution) and extend its domain of analyticity we follow Ref. [36], whose method is based on the original work of [37–40], and introduce the following conformal

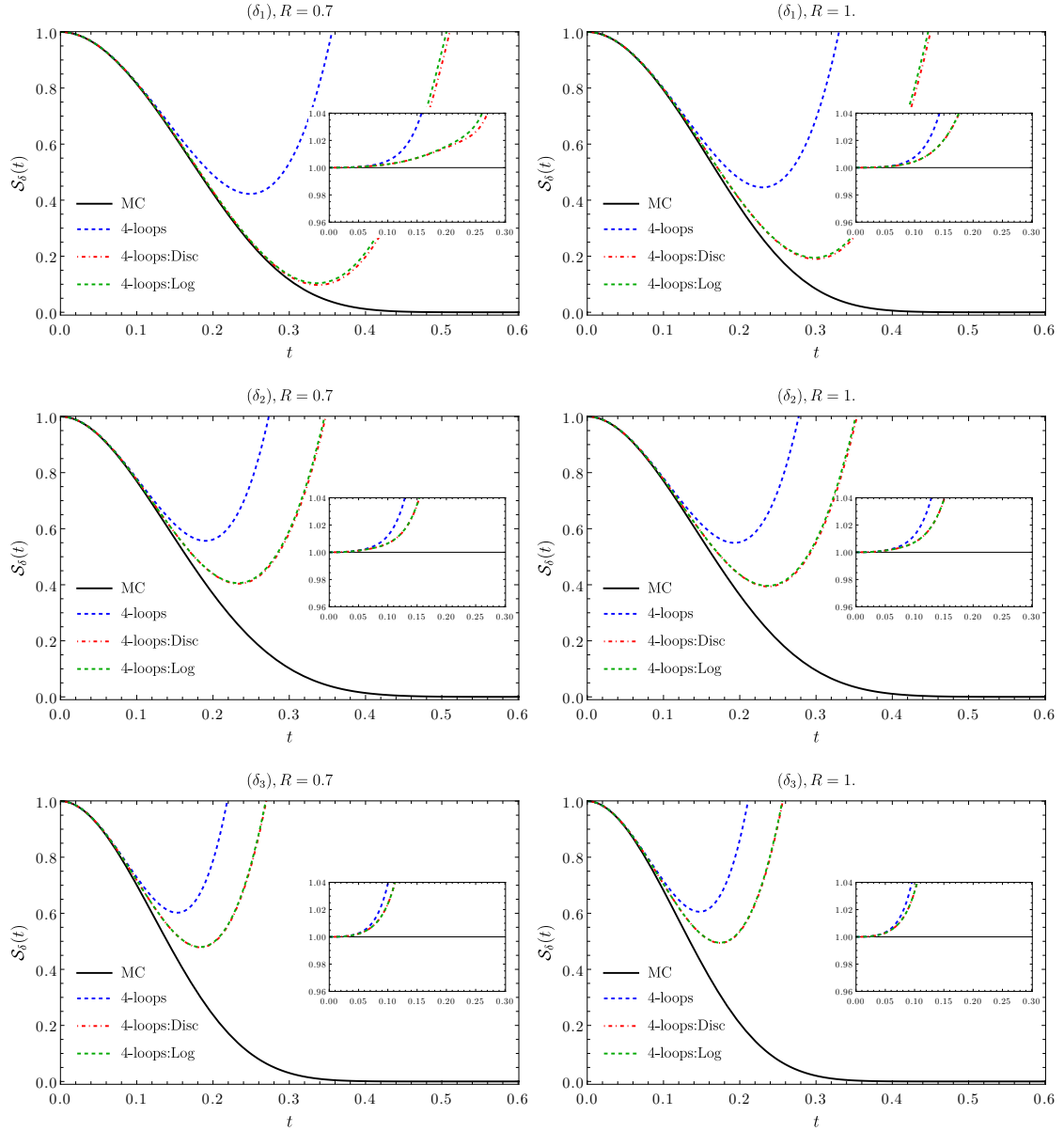


Figure 10: Comparisons between the all-orders large- N_c MC result and the series expansion up to 4-loops with and without conformal improvement for both $R = 0.7$ and $R = 1.0$ and for all Born channels.

transformations:

$$t \rightarrow u(t) = \begin{cases} \frac{\sqrt{1+t}-1}{\sqrt{1+t+1}}, \\ \log(1+t). \end{cases} \quad (4.5)$$

The transformation in the first line, referred to as *disc mapping*, maps the t plane to a disc, while the other transformation, referred to as *log mapping*, was derived in [36] based on the dressed gluon expansion technique. Notice that $u(0) = 0$ for both transformations.

This is a necessary condition for conformal mappings. Moreover, from Eq. (4.5) we infer the inverse relations: $t = 4u/(1-u)^2$ and $t = e^u - 1$. To apply the said transformations we first substitute for the parameter t in the expansion of Eq. (4.4) by the latter expressions, power expand in terms of u and then substitute back for u the expressions in (4.5).

In Fig. 10 we compare the NGLs series expansion up to 4-loops with and without conformal improvements against the numerical MC distribution. We observe that both disc and log mappings perform equally well in improving the convergence of the power series. For instance, for channel (δ_1) excellent agreement is achieved for up to $t \sim 0.3$ and $t \sim 0.2$ for $R = 0.7$ and $R = 1.0$, respectively. This is almost the double of that seen for the expansion without conformal improvement. Nevertheless, the conformal improvement seems to vary noticeably with the Born channel and slightly with the jet radius, performing worst for channel (δ_3) and $R = 1.0$. It is worth noting, as stated in [36], that conformal mappings are a form of resummation only captured in a purely algebraic form, hence they allow for a larger radius of convergence when compared to fixed-order expansions.

Another possible way to further improve the convergence of the series expansion is to apply the conformal mapping to the logarithm of the expansion distribution and then exponentiate it again (as the exponentiation cancels out the logarithm) [36]. In Fig. 11 we show comparisons between the all-orders MC distribution and the said conformal improvement of the logarithm of the series expansion. Excellent agreement is evident for quite large values of t extending to about $t \sim 0.4$ and beyond for some cases. This is a significant improvement compared to the original series expansion shown in Fig. 9. It is comparable to, or even better in many cases than, the exponential form plotted in Fig. 7.

5 Conclusion

In this paper, we have computed, for the first time in the literature, the distribution of NGLs up to 4-loops in processes involving a Higgs/vector boson + a single hard jet at hadron colliders. Our calculations focus on the invariant mass of the leading hard jet using the anti- k_t jet algorithm. They are valid in the eikonal (soft) limit with strong-energy ordering, accurate to single logarithmic accuracy, and incorporate the full colour (finite- N_c) and jet radius R dependencies of the various NGL coefficients.

Calculations at 2- and 3-loops have been performed analytically, including explicit R dependence. We demonstrate that as $R \rightarrow 0$, NGL coefficients at these loop orders converge to those observed in the e^+e^- hemisphere mass distribution. However, computation of 4-loop coefficients involves partial numerical methods due to complexities arising from quadrupole ghost terms in squared eikonal amplitudes. These terms exhibit distinctive features, leading to the non-trivial observation that the e^+e^- results are not fully recovered in the $R \rightarrow 0$ limit for 4-loop coefficients, contrasting with 2- and 3-loops results.

Comparison with all-orders large- N_c numerical results reveals that incorporating higher-loop NGL coefficients improves agreement with numerical MC simulations, particularly for small values of the evolution parameter t (around $t \lesssim 0.15$). Notably, 2- and 4-loop results outperform the 3-loop results in capturing the overall shape of the MC curve. The performance is less satisfactory for the series expansion of the NGLs resummed form factor,

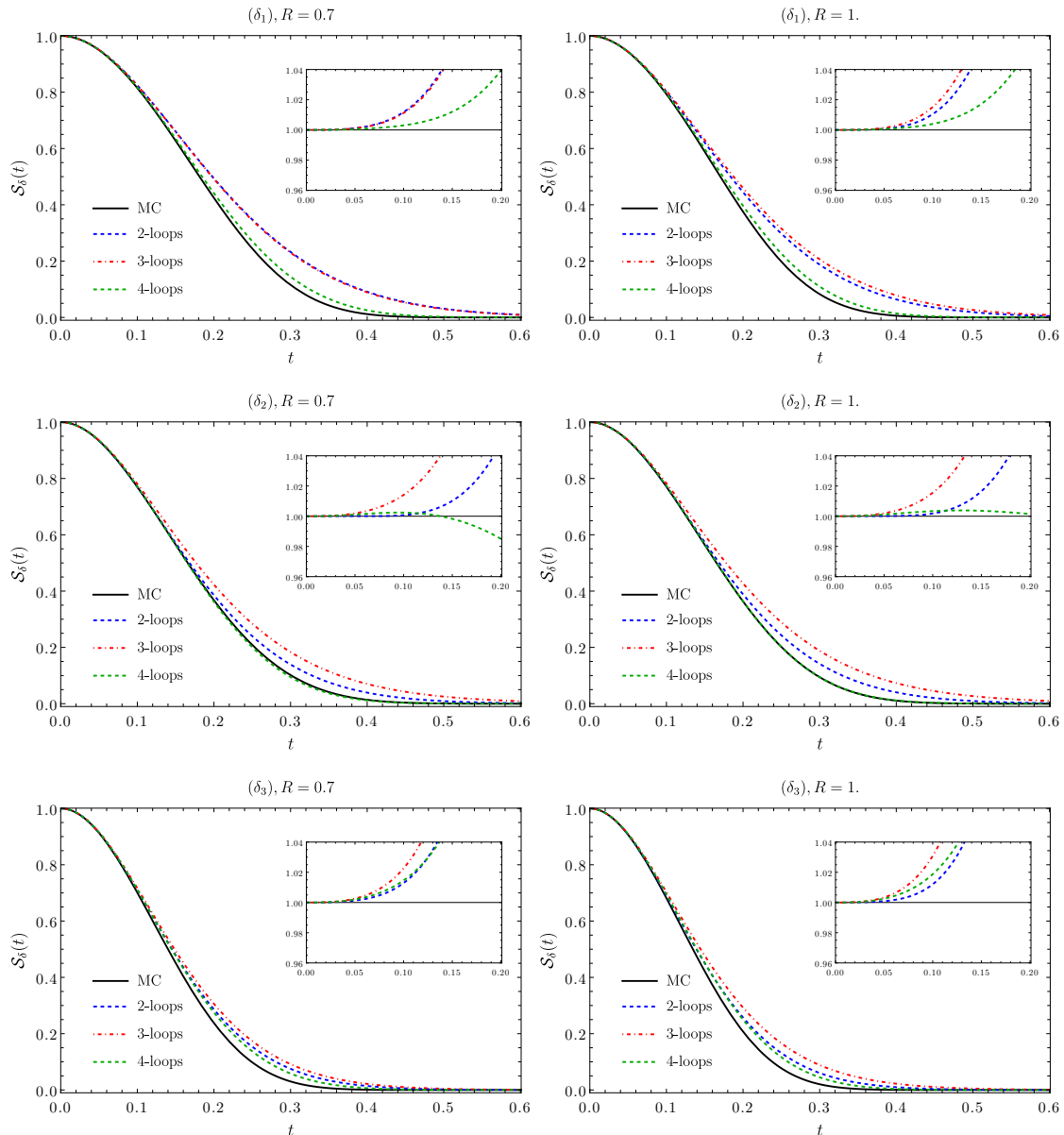


Figure 11: Comparisons between the all-orders large- N_c MC result and the conformally improved logarithm of the analytical series expansion of (4.3) for both $R = 0.7$ and $R = 1.0$ and for all Born channels,

indicating a convergence radius around $t \sim 0.17$, consistent with previous findings. One way to improve this convergence is to use conformal transformations, which are a type of resummation. The resultant conformally improved analytical distributions show excellent agreement with the all-orders solution over a large range of values of the evolution parameter t , thus proving the importance of such transformations for accurate studies.

Furthermore, we have found that the overall features observed for NGLs calculations in e^+e^- collisions extend to hadronic V/H+jet processes. This includes, for instance, the

significance of finite- N_c contributions and the impact of jet radius in the phenomenological studies of jet shapes. Whether the same also applies for hadronic $2 \rightarrow 2$ scattering processes will be investigated in the near future.

Acknowledgement

I would like to thank Y. Delenda for valuable discussions, insightful comments, and for reviewing the manuscript.

A 4-loops calculations

In this appendix we present the details of the 4-loops calculations. The integral expressions of the terms mentioned in Eq. (3.28) are given by:

$$\mathcal{K}_{\alpha\beta}^{(1)} = R^8 \int_0^{2\pi} \prod_{i=1}^4 \frac{d\theta_i}{2\pi} \int_1^{\frac{\pi}{R|\sin\theta_1|}} r_1 dr_1 \int_0^1 \prod_{j=2}^4 r_j dr_j \mathcal{A}_{\alpha\beta}^{12} \bar{\mathcal{A}}_{\alpha\beta}^{13} \bar{\mathcal{A}}_{\alpha\beta}^{14}, \quad (\text{A.1a})$$

$$\mathcal{K}_X^{(2)} = R^8 \int_0^{2\pi} \prod_{i=1}^4 \frac{d\theta_i}{2\pi} \int_1^{\frac{\pi}{R|\sin\theta_1|}} r_1 dr_1 \int_0^1 \prod_{j=2}^4 r_j dr_j \bar{\mathcal{N}}_{1234}^{\text{RVVR}}, \quad (\text{A.1b})$$

$$\mathcal{K}_{\alpha\beta}^{(3)} = R^8 \int_0^{2\pi} \prod_{i=1}^4 \frac{d\theta_i}{2\pi} \prod_{j=1,3} \int_1^{\frac{\pi}{R|\sin\theta_j|}} r_j dr_j \int_0^1 \prod_{\ell=2,4} r_\ell dr_\ell \mathcal{A}_{\alpha\beta}^{12} \bar{\mathcal{B}}_{\alpha\beta}^{134}, \quad (\text{A.1c})$$

$$\mathcal{K}_X^{(4)} = R^8 \int_0^{2\pi} \prod_{i=1}^4 \frac{d\theta_i}{2\pi} \prod_{j=1,3} \int_1^{\frac{\pi}{R|\sin\theta_j|}} r_j dr_j \int_0^1 \prod_{\ell=2,4} r_\ell dr_\ell (\bar{\mathcal{N}}_{1234}^{\text{RVVR}} + \bar{\mathcal{N}}_{1234}^{\text{RVRR}}), \quad (\text{A.1d})$$

$$\mathcal{K}_{\alpha\beta}^{(5)} = R^8 \int_0^{2\pi} \prod_{i=1}^4 \frac{d\theta_i}{2\pi} \prod_{j=1,2} \int_1^{\frac{\pi}{R|\sin\theta_j|}} r_j dr_j \int_0^1 \prod_{\ell=3,4} r_\ell dr_\ell (\mathcal{A}_{\alpha\beta}^{13} \bar{\mathcal{B}}_{\alpha\beta}^{124} + \mathcal{A}_{\alpha\beta}^{14} \bar{\mathcal{B}}_{\alpha\beta}^{123}), \quad (\text{A.1e})$$

$$\mathcal{K}_{\alpha\beta}^{(6)} = R^8 \int_0^{2\pi} \prod_{i=1}^4 \frac{d\theta_i}{2\pi} \prod_{j=1,2} \int_1^{\frac{\pi}{R|\sin\theta_j|}} r_j dr_j \int_0^1 \prod_{\ell=3,4} r_\ell dr_\ell \mathfrak{A}_{\alpha\beta}^{1234}, \quad (\text{A.1f})$$

$$\mathcal{K}_{\alpha\beta}^{(7)} = R^8 \int_0^{2\pi} \prod_{i=1}^4 \frac{d\theta_i}{2\pi} \prod_{j=1,2} \int_1^{\frac{\pi}{R|\sin\theta_j|}} r_j dr_j \int_0^1 \prod_{\ell=3,4} r_\ell dr_\ell \mathbf{A}_{\alpha\beta}^{1234}, \quad (\text{A.1g})$$

$$\mathcal{K}_X^{(8)} = R^8 \int_0^{2\pi} \prod_{i=1}^4 \frac{d\theta_i}{2\pi} \prod_{j=1,2} \int_1^{\frac{\pi}{R|\sin\theta_j|}} r_j dr_j \int_0^1 \prod_{\ell=3,4} r_\ell dr_\ell (\bar{\mathcal{N}}_{1234}^{\text{RVVR}} + \bar{\mathcal{N}}_{1234}^{\text{RRVR}}), \quad (\text{A.1h})$$

$$\mathcal{K}_{\alpha\beta}^{(9)} = R^8 \int_0^{2\pi} \prod_{i=1}^4 \frac{d\theta_i}{2\pi} \prod_{j=1,2,3} \int_1^{\frac{\pi}{R|\sin\theta_j|}} r_j dr_j \int_0^1 r_4 dr_4 \mathcal{C}_{\alpha\beta}^{1234}, \quad (\text{A.1i})$$

where the various angular functions are given in Ref. [29]. Since the integration of some the above integrals, particularly the quadrupole ghost terms and the terms involving the jet parton as one of the dipole legs, have proven to be analytically formidable we shall confine ourselves to just provide the numerical values of the integrations. They are reported in Table 1. Notice that $\mathcal{K}_{(ij)}^{(5)} = 2\mathcal{K}_{(ij)}^{(3)}$ and thus will not be shown explicitly in the latter table.

R	$\mathcal{K}_{ij}^{(1)}$		$\mathcal{K}_X^{(2)}$	$\mathcal{K}_{ij}^{(3)}$		$\mathcal{K}_X^{(4)}$	$\mathcal{K}_{ij}^{(6)}$		$\mathcal{K}_{ij}^{(7)}$		$\mathcal{K}_X^{(8)}$	$\mathcal{K}_{ij}^{(9)}$	
	$\mathcal{K}_{aj}^{(1)}$	$\mathcal{K}_{ab}^{(1)}$		$\mathcal{K}_{aj}^{(3)}$	$\mathcal{K}_{ab}^{(3)}$		$\mathcal{K}_{aj}^{(6)}$	$\mathcal{K}_{ab}^{(6)}$	$\mathcal{K}_{aj}^{(7)}$	$\mathcal{K}_{ab}^{(7)}$		$\mathcal{K}_{aj}^{(9)}$	$\mathcal{K}_{ab}^{(9)}$
0.	3.25	0.	0.	0.474	0.	0.	1.15	0.	0.271	0.	2.7	1.29	0.
0.1	3.25	0.032	-0.015	0.461	0.017	0.01	1.15	0.076	0.275	0.001	2.64	1.25	0.177
0.2	3.25	0.129	-0.059	0.462	0.060	0.035	1.15	0.212	0.29	0.010	2.51	1.25	0.373
0.3	3.25	0.287	-0.131	0.464	0.12	0.069	1.15	0.363	0.315	0.037	2.37	1.27	0.557
0.4	3.25	0.5	-0.229	0.465	0.187	0.106	1.15	0.509	0.348	0.087	2.22	1.12	0.689
0.5	3.26	0.759	-0.35	0.466	0.255	0.147	1.15	0.641	0.391	0.165	2.1	1.17	0.903
0.6	3.27	1.06	-0.492	0.454	0.319	0.177	1.15	0.759	0.441	0.27	1.99	1.21	1.11
0.7	3.28	1.38	-0.651	0.456	0.376	0.208	1.16	0.859	0.499	0.4	1.9	1.21	1.26
0.8	3.31	1.72	-0.832	0.477	0.433	0.235	1.16	0.954	0.268	0.552	1.84	1.2	1.44
0.9	3.34	2.07	-1.03	0.461	0.471	0.266	1.16	1.05	0.277	0.719	1.8	1.19	1.56
1.	3.4	2.42	-1.25	0.48	0.504	0.285	1.17	1.14	0.295	0.899	1.77	1.19	1.74
1.1	3.47	2.75	-1.5	0.472	0.533	0.303	1.18	1.23	0.322	1.08	1.76	1.21	1.88
1.2	3.56	3.08	-1.77	0.496	0.556	0.316	1.2	1.33	0.358	1.27	1.76	1.22	2.03

Table 1: Numerical values of the various 4-loops NGLs integrals.

References

- [1] K. Khelifa-Kerfa and Y. Delenda, *Non-global logarithms at finite N_c beyond leading order*, *JHEP* **03** (2015) 094 [[1501.00475](#)].
- [2] R. Kogler et al., *Jet Substructure at the Large Hadron Collider: Experimental Review*, *Rev. Mod. Phys.* **91** (2019) 045003 [[1803.06991](#)].
- [3] A.J. Larkoski, I. Moult and B. Nachman, *Jet Substructure at the Large Hadron Collider: A Review of Recent Advances in Theory and Machine Learning*, *Phys. Rept.* **841** (2020) 1 [[1709.04464](#)].
- [4] M. Dasgupta and G.P. Salam, *Resummation of nonglobal QCD observables*, *Phys. Lett. B* **512** (2001) 323 [[hep-ph/0104277](#)].
- [5] M. Dasgupta and G.P. Salam, *Accounting for coherence in interjet $E(t)$ flow: A Case study*, *JHEP* **03** (2002) 017 [[hep-ph/0203009](#)].
- [6] M. Dasgupta and G.P. Salam, *Resummed event shape variables in DIS*, *JHEP* **08** (2002) 032 [[hep-ph/0208073](#)].
- [7] A. Banfi, G. Marchesini and G. Smye, *Away from jet energy flow*, *JHEP* **08** (2002) 006 [[hep-ph/0206076](#)].
- [8] R.B. Appleby and M.H. Seymour, *Nonglobal logarithms in interjet energy flow with k_t clustering requirement*, *JHEP* **12** (2002) 063 [[hep-ph/0211426](#)].
- [9] J.R. Forshaw, A. Kyrieleis and M.H. Seymour, *Super-leading logarithms in non-global observables in QCD*, *JHEP* **08** (2006) 059 [[hep-ph/0604094](#)].
- [10] A. Banfi, M. Dasgupta, K. Khelifa-Kerfa and S. Marzani, *Non-global logarithms and jet algorithms in high- p_T jet shapes*, *JHEP* **08** (2010) 064 [[1004.3483](#)].

- [11] K. Khelifa-Kerfa, *Non-global logs and clustering impact on jet mass with a jet veto distribution*, *JHEP* **02** (2012) 072 [[1111.2016](#)].
- [12] M. Dasgupta, K. Khelifa-Kerfa, S. Marzani and M. Spannowsky, *On jet mass distributions in Z +jet and dijet processes at the LHC*, *JHEP* **10** (2012) 126 [[1207.1640](#)].
- [13] Y. Delenda and K. Khelifa-Kerfa, *On the resummation of clustering logarithms for non-global observables*, *JHEP* **09** (2012) 109 [[1207.4528](#)].
- [14] M.D. Schwartz and H.X. Zhu, *Nonglobal logarithms at three loops, four loops, five loops, and beyond*, *Phys. Rev. D* **90** (2014) 065004 [[1403.4949](#)].
- [15] A. Banfi, F.A. Dreyer and P.F. Monni, *Next-to-leading non-global logarithms in QCD*, *JHEP* **10** (2021) 006 [[2104.06416](#)].
- [16] A. Banfi, F.A. Dreyer and P.F. Monni, *Higher-order non-global logarithms from jet calculus*, *JHEP* **03** (2022) 135 [[2111.02413](#)].
- [17] M. Cacciari, G.P. Salam and G. Soyez, *The anti- k_t jet clustering algorithm*, *JHEP* **04** (2008) 063 [[0802.1189](#)].
- [18] S. Catani, Y.L. Dokshitzer, M.H. Seymour and B.R. Webber, *Longitudinally invariant K_t clustering algorithms for hadron hadron collisions*, *Nucl. Phys. B* **406** (1993) 187.
- [19] S.D. Ellis and D.E. Soper, *Successive combination jet algorithm for hadron collisions*, *Phys. Rev. D* **48** (1993) 3160 [[hep-ph/9305266](#)].
- [20] Y.L. Dokshitzer, G.D. Leder, S. Moretti and B.R. Webber, *Better jet clustering algorithms*, *JHEP* **08** (1997) 001 [[hep-ph/9707323](#)].
- [21] N. Ziani, K. Khelifa-Kerfa and Y. Delenda, *Jet mass distribution in Higgs/vector boson + jet events at hadron colliders with k_t clustering*, *Eur. Phys. J. C* **81** (2021) 570 [[2104.11060](#)].
- [22] R. Gauld, A. Gehrmann-De Ridder, E.W.N. Glover, A. Huss and I. Majer, *VH + jet production in hadron-hadron collisions up to order α_s^3 in perturbative QCD*, *JHEP* **03** (2022) 008 [[2110.12992](#)].
- [23] R. Boughezal, C. Focke, W. Giele, X. Liu and F. Petriello, *Higgs boson production in association with a jet at NNLO using jetiness subtraction*, *Phys. Lett. B* **748** (2015) 5 [[1505.03893](#)].
- [24] R. Boughezal, J.M. Campbell, R.K. Ellis, C. Focke, W.T. Giele, X. Liu et al., *Z-boson production in association with a jet at next-to-next-to-leading order in perturbative QCD*, *Phys. Rev. Lett.* **116** (2016) 152001 [[1512.01291](#)].
- [25] A. Gehrmann-De Ridder, T. Gehrmann, E.W.N. Glover, A. Huss and T.A. Morgan, *The NNLO QCD corrections to Z boson production at large transverse momentum*, *JHEP* **07** (2016) 133 [[1605.04295](#)].
- [26] R. Boughezal, X. Liu and F. Petriello, *W-boson plus jet differential distributions at NNLO in QCD*, *Phys. Rev. D* **94** (2016) 113009 [[1602.06965](#)].
- [27] A. Gehrmann-De Ridder, T. Gehrmann, E.W.N. Glover, A. Huss and T.A. Morgan, *Precise QCD predictions for the production of a Z boson in association with a hadronic jet*, *Phys. Rev. Lett.* **117** (2016) 022001 [[1507.02850](#)].
- [28] J.M. Campbell, R.K. Ellis and C. Williams, *Driving missing data at the LHC: NNLO predictions for the ratio of $\gamma + j$ and $Z + j$* , *Phys. Rev. D* **96** (2017) 014037 [[1703.10109](#)].

- [29] K. Khelifa-Kerfa and Y. Delenda, *Eikonal amplitudes for three-hard legs processes at finite- N_c* , *Phys. Lett. B* **809** (2020) 135768 [[2006.08758](#)].
- [30] Y. Delenda and K. Khelifa-Kerfa, *Eikonal gluon bremsstrahlung at finite N_c beyond two loops*, *Phys. Rev. D* **93** (2016) 054027 [[1512.05401](#)].
- [31] T. Hahn, *CUBA: A Library for multidimensional numerical integration*, *Comput. Phys. Commun.* **168** (2005) 78 [[hep-ph/0404043](#)].
- [32] T. Hahn, *Concurrent Cuba*, *Comput. Phys. Commun.* **207** (2016) 341.
- [33] K. Khelifa-Kerfa, “NGLs up to 4-loops for V/H+jet processes in k_t algorithm.” in progress.
- [34] A. Banfi, G.P. Salam and G. Zanderighi, *Principles of general final-state resummation and automated implementation*, *JHEP* **03** (2005) 073 [[hep-ph/0407286](#)].
- [35] S. Caron-Huot, “Note on perturbative solution to the BMS equation.” private communication.
- [36] A.J. Larkoski, I. Moult and D. Neill, *The Analytic Structure of Non-Global Logarithms: Convergence of the Dressed Gluon Expansion*, *JHEP* **11** (2016) 089 [[1609.04011](#)].
- [37] G. Altarelli, P. Nason and G. Ridolfi, *A Study of ultraviolet renormalon ambiguities in the determination of alpha-s from tau decay*, *Z. Phys. C* **68** (1995) 257 [[hep-ph/9501240](#)].
- [38] I. Caprini and J. Fischer, *Convergence of the expansion of the Laplace-Borel integral in perturbative QCD improved by conformal mapping*, *Phys. Rev. D* **62** (2000) 054007 [[hep-ph/0002016](#)].
- [39] I. Caprini and J. Fischer, *Determination of $\alpha_s(M_\tau^2)$: a conformal mapping approach*, *Nucl. Phys. B Proc. Suppl.* **218** (2011) 128 [[1011.6480](#)].
- [40] J. Zinn-Justin, *Quantum field theory and critical phenomena*, *Int. Ser. Monogr. Phys.* **113** (2002) 1.